

Dykes, cups, saucers and sills: Analogue experiments on magma intrusion into brittle rocks

L. Mathieu^{a,b,*}, B. van Wyk de Vries^a, Eoghan P. Holohan^b, Valentin R. Troll^{b,c}

^a *Laboratoire Magmas et Volcans, Observatoire de Physique du Globe de Clermont, Université Blaise Pascal, 5 rue Kessler, 63038 Clermont-Ferrand, France*

^b *Department of Geology, Trinity College Dublin, Dublin 2, Ireland*

^c *Department of Earth Sciences, Uppsala University, Villavägen 16, SE-752 36 Uppsala, Sweden*

Received 27 August 2007; received in revised form 29 December 2007; accepted 8 February 2008

Available online 4 March 2008

Editor: C.P. Jaupart

Abstract

Magma is transported in the crust by blade-like intrusions such as dykes, sills, saucers, and also collects in thicker laccoliths, lopoliths and plutons. Recently, the importance and great number of shallow (<5 km) saucer-shaped intrusions has been recognized. Lopoliths and cup-shaped intrusions have also been reported in many geological contexts. Our field observations indicate that many intrusions, especially those emplaced into breccias or fractured rocks, have bulging, lobate margins and have shear faults at their bulbous terminations. Such features suggest that magma can propagate along a self-induced shear fault rather than a hydraulic tension-fracture. To investigate this we use analogue models to explore intrusion propagation in a brittle country rock. The models consist of the injection of analogue magma (honey or Golden syrup) in a granular material (sand or sieved ignimbrite) that is a good analogue for brittle or brecciated rocks. These models have the advantage (over other models that use gelatin) to well represent the properties of brittle materials by allowing both shear-faults and tension fractures to be produced at suitable stresses. In our experiments we mainly obtain vertical dykes and inverted-cone like structures that we call cup-shaped intrusions. Dykes bifurcate into cup-shaped intrusions at depths depending on their viscosity. All cup-shaped intrusions uplift a central block. By injecting against a vertical glass plate we obtain detailed observations of the intrusion propagation style. We observe that dykes commonly split and produce cup-shaped intrusions near the surface and that shear zone-related intrusions develop at the dyke tip. We conclude that many dykes propagate as a viscous indenter resulting from shear failure of host rock rather than tensional hydraulic fracturing of host rocks. The shear propagation model provides an explanation for the shape and formation of cup-shaped intrusions, saucer-sills and lopoliths.

© 2008 Published by Elsevier B.V.

Keywords: dykes; magma; cup-shaped-intrusions; analogue models; viscous indenter

1. Introduction

Recently, hundreds of saucer-shaped intrusions have been discovered in sedimentary basins (Chevallier and Woodford, 1999; Hansen and Cartwright, 2006). In addition, some magmatic complexes traditionally thought of as ring-dykes are beginning to be reinterpreted as lopoliths or inverted cone-shaped intrusive

systems (e.g. O'Driscoll et al., 2006). In addition, similar intrusions could underlie ring-like volcanic complexes such as those common in the in the Andes (e.g. Klemetti and Grunder, 2008). Thus, it has become clear that inverted-cone-shaped intrusions may be an important way of holding and transporting magma through the crust. Analogue models involving low viscosity liquid intrusions into coulomb materials have been developed by Galland et al. (2006). These show that the use of low viscosity liquids and of a brittle analogue material can create realistic scaled models for magma intrusion. Here, we investigate the mechanism and geometry of intrusions into brittle crust with an adapted analogue model and provide field observations.

* Corresponding author. Laboratoire Magmas et volcans, Observatoire du Physique du Globe de Clermont, Université Blaise Pascal, 5 rue Kessler, 63038 Clermont-Ferrand, France. Tel.: +33 473346700; fax: +33 473346744.

E-mail address: lassolas@free.fr (L. Mathieu).

URL: <http://www.opgc.univ-bpclermont.fr/> (L. Mathieu).

The aim of our experiments is to model shallow-level intrusions, especially dykes and saucer- or cup-shaped bodies. Previously, the propagation of dykes and other small-scale intrusions has been extensively studied using gelatin models. Gelatin fails in tension, but it is too cohesive to fully represent weak brittle rocks. Here, we have chosen to model host rocks by a granular material that can fail both in tension and, at low differential stresses, by shear failure. We performed two sets of experiments using different setups and analogue materials.

1.1. Classification and terminology of intrusion geometry

Most crustal intrusions are dykes or sills: sheet-shaped bodies with a thickness of several meters and lengths of meters up to kilometers. Thicker intrusions include stocks, cryptodomes, laccoliths and plutons, as well as lopoliths and the recently described saucers. The range of shapes described and the different possible genetic relationships make a classification of shapes difficult. Also certain terms, such as cone-sheet, have a genetic connotation, related to specific model-driven interpretations. For this reason we propose the following classification of forms.

Dykes are steep, generally cross-cutting intrusions (Fig. 1a). Cone-sheets can be dykes organized in swarms of many arcuate intrusions that dip inward toward a focal point (Fig. 1b). Such intrusions may be associated with, and fed from several kinds of intrusions that are large-scale accumulations of magma in the crust. Such magmatic accumulations have variable morphology, ranging from thick dykes to cup-shaped intrusions (Fig. 1c), saucer-shaped intrusions (Fig. 1d) and sills (Fig. 1e). They may be thicker to take on a lopolith shape (Fig. 1f). Intermediate shapes are spherical or disk-shaped plutons (Fig. 1g). The opposite geometry to a lopolith is a laccolith (Fig. 1h) and to a cup-shaped intrusion is a ring-dyke, with a bell-jar shape as a possible end member (Fig. 1i). While the general shape ratio of large and deep intrusions is constrained (Petford et al., 2000), their exact morphology is more difficult to estimate and could be laccolithic, lopolithic, lens or possibly cup-shaped. We note

that there are thin (dyke like) and thick (pluton like) intrusions, and that the two may have different modes of growth: by crack opening and infiltration (dykes) and wall rock displacement/deformation (thick ‘plutonic’ intrusions).

1.2. Mechanisms of intrusion emplacement

Pioneering work by Pollard (1973) on intrusion mechanisms suggested that there are several ways to intrude magma in the crust. The consensus has grown toward considering hydraulic fracturing as the principle mechanism for intrusion propagation. Brittle rocks can fail in tension under the pressure exerted by magma and fluid-filled fractures form (Hubbert and Willis, 1957; Jaeger, 1972). The hydraulic fracturing of rocks is the only mechanism that propagates magma fast enough before its complete solidification according to Spence and Turcotte (1990). However, many intrusions are emplaced in fault zones (Morris and Hutton, 1993) and there are examples of intrusions propagating with associated brittle and ductile faulting (Pollard, 1973). Pollard (1973) suggested that dykes can be emplaced by three main mechanisms: tensional fracturing (shallow-depth intrusion splits the host rocks and propagates in the tensional fracture), brittle faulting (deeper intrusions propagate into the brittle faults that form at their termination) and ductile faulting (at high confining pressure and high temperature, ductile faulting occurs near the termination and the intrusion grows by displacing the host rock).

Dyke propagation by fracturing has been modeled by numerical and analogue models (Pollard, 1973; Hyndman and Alt, 1987; Spence and Turcotte, 1990; Lister and Kerr, 1991; Heimpel and Oison, 1994; Takada, 1994). The analogue models consist in the injection of a liquid into gelatin. The resulting intrusions are sheet-shaped and propagate by coalescence of liquid-filled buoyancy-driven fractures and pressure cracks (Takada, 1994).

The propagation direction of sheet intrusions is mainly controlled by the regional stress orientation, by the presence of planar discontinuities, such as pre-existing fractures and faults, by compositional layering in the host rock and by changes in the properties of host rocks (Pollard, 1973). None of the above has been modeled here. In order to simplify the models, analogue liquid was injected in a homogeneous medium.

2. Analogue modelling

2.1. Materials

2.1.1. Country rock

In the experiments presented here, country rocks are represented by a granular material. A first set of experiments was carried out with sand and a second set with fine-grained ignimbrite powder. These materials have slightly different densities, angles of internal friction and cohesions (Table 1). Sand is a Coulomb material that fails in shear and is suitable for modelling deformation of the upper crust (Hubbert, 1937; Schellart, 2000). Initially, sand was used as the normal laboratory standard but was replaced by ignimbrite that allows less infiltration from the intruded magma analogue. This material is sieved Grande Nappe Ignimbrite, from Mont Dore volcano, France. It consists of glass

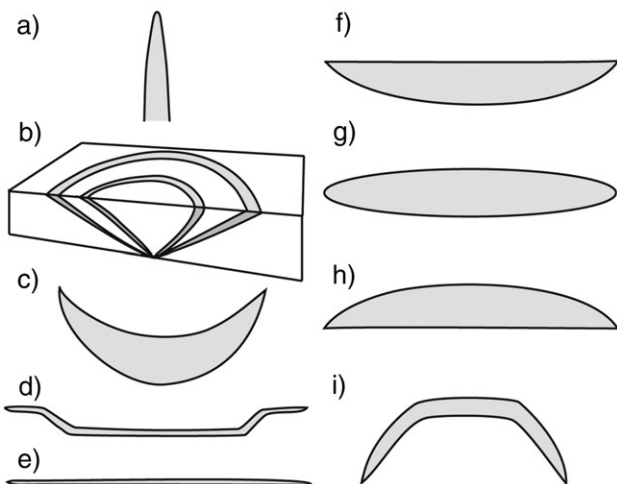


Fig. 1. The shape classification of magmatic intrusions: (a) dyke (b) cone-sheet (c) cup-shaped intrusion (d) saucer-shaped intrusion (e) sill (f) lopolith (g) pluton (h) laccolith (i) ring dyke.

Table 1
Experimental variables and their values in experiments compared with natural values

Parameters	Dimension	Definition	Value		
			Nature (N)	Model (M)	Ratio* (M/N)
H	m	Length scale (country rock depth)	100	0.1	10^{-3}
P	kg m^{-3}	density of country rocks	2800	1400	0.5
ρ_i	kg m^{-3}	density of intrusions	2800	1400	0.5
G	m s^{-2}	gravity acceleration	9.81	9.81	1
σ	Pa	cohesion of country rocks	2×10^5	100	$5 \cdot 10^{-4}$
Φ		frictional angle of country rocks	30°	30°	1
v_d	m s^{-1}	velocity of intrusion propagation	0.2	$2 \cdot 10^{-5}$	10^{-4}
t	s	time			10
μ	Pa s	viscosity of intrusion	10^4	50	$5 \cdot 10^{-3}$
v_i	m s^{-1}	intrusion rate (flux)	10	10^{-9}	10^{-10}
P	Pa	overpressure	$4 \cdot 10^6$	2000	$5 \cdot 10^{-4}$
Π_1	–	H_{intr}/Φ	0.3	0.2–0.3	~ 1
Π_2	–	$H_{\text{base}}/H_{\text{max}}$	0.05–0.5	0.06–0.5	~ 1
Π_3	–	Φ/H_{max}	0.05–0.5	0.04–0.5	~ 1
Π_4	–	$\mu/[(H_{\text{max}})^{3/2} \rho^* (g)^{1/2}]$	0.1–0.2	0.1–0.4	~ 1

In each case a standard value is chosen for the scaling. For certain values this remained constant, such as for density, or varied by small amounts (angle of internal friction). For other parameters values varied, such as viscosity that was varied from 50 to 200 Pa s, corresponding to magmas with 10^4 to 10^5 Pa s viscosity. Analogue intrusion velocities varied from 1.7×10^{-5} to 9×10^{-5} ms^{-1} , and fluxes from 10^{-8} m^3s^{-1} to 10^{-9} m^3s^{-1} . A selection of the dimensionless numbers established for the experiments is also given. The ranges given corresponds to the variability in natural examples and those in the analogue materials.

and quartz grains less than 250 μm in diameter. The sand used in the first set of experiments has a low cohesion (0 to 10 Pa). Its angle of internal friction is 30° . The ignimbrite used in the subsequent experiments is more cohesive (100 to 230 Pa), with a similar angle of internal friction (38°). Smallest grains are about 1 μm , and these effectively block the pore spaces in the powder. The ignimbrite powder is more cohesive (100–230 Pa) than sand (0–10 Pa) and it can fail both in tension and when confined, fails with shear band formation, like other granular materials.

2.1.2. Magma

The analogue materials for magma are honey and Golden syrup. First we used honey at various temperatures to test a range of viscosities: the honey used is 80 Pa s at 50°C , 140 Pa s at 35°C and 200 Pa s at 22°C . Subsequently, we used Golden syrup (Tate and Lyle's Golden syrup) for an analogue, as it is more stable, easier to handle and cheaper than honey. Golden syrup has a viscosity of 50 Pa s at 22°C . The liquid used represents a basaltic to intermediate magma with moderate viscosity between 10^4 and 10^5 Pa s.

2.2. Scaling

We scale our models (Table 1) following methodology developed by Ramberg (1981), Merle and Borgia (1996), Donnadieu and Merle (1998), Cecchi et al. (2004). The length

ratio defined by the depth of the models and thickness of natural rocks (H^*) is initially taken as 10^{-3} (1 cm represents 10 m).

The average grain size of sand is 200–300 μm and is 10–250 μm for ignimbrite. Pore sizes are linearly related to grain size. Thus, according to our scaling, the grain and pore sizes in nature are 2–3 mm and 0.1–2.5 mm.

The ratio between the density of sand in experiments and estimated natural density (ρ^*) is about 0.5. As gravity is the same in our experiments and in nature ($g^*=1$), the stress ratio is calculated from:

$$\sigma^* = \rho^* \cdot g^* \cdot H^* = 5 \times 10^{-4} \quad (1)$$

Sand and ignimbrite models should be thus about 10^4 times weaker than a natural example. The sand thus represents a slightly weaker country rock than the ignimbrite with the sand scaling to about 10^4 Pa and the ignimbrite powder to 10^5 Pa. These values are similar to those estimated for breccias in volcanoclastic rocks (Voight, 2000).

To scale viscosity we first consider time, through the velocity of intrusion. Estimates of the upper propagation velocity of natural intrusions range from 0.5 m s^{-1} (Spence and Turcotte, 1985) to 1 m s^{-1} (Heimpel and Oison, 1994). We consider, for scaling, natural intrusions with a lower average propagation velocity of 0.1 m s^{-1} . The model intrusions propagate at about $1 \times 10^{-5} \text{ m s}^{-1}$, so the velocity ratio vd^* is, 10^{-4} .

Thus, using the length ratio, we can define the time ratio:

$$t^* = H^*/vd^* = 10 \quad (2)$$

The viscosity ratio can also be defined as follows:

$$\sigma^* \cdot t^* = \mu^* = 5 \times 10^{-3} \quad (3)$$

Thus we find that our standard model liquids corresponds to a magma that has a viscosity of 10^4 Pa s. The viscosity is that of basaltic or basaltic andesite magma with low to moderate crystal contents.

The scaling can be modified to take different length scales, viscosity scales and timescales into account (e.g. Donnadieu and Merle, 1998; Holohan et al., 2007). For different natural viscosity values, scaling provides a corresponding value of H^* (Fig. 2). For example, if we consider an acid magma or crystalline basic magma with a viscosity of 10^6 Pa s, the value of the length ratio is 1.3×10^{-6} (1 cm=7.5 km). Using this procedure, our models may be applied to various magmas, intrusion depths, sizes and geological settings. For example a small dyke of basaltic magma in breccia relates to the basic scaling presented above. A large semi-solidified pluton with high crystal content would relate to the higher viscosity scaling. An important caveat is that at large scales, lower viscosity magmas certainly co-exist with high viscosity intrusions and these would create structures that we cannot model. However, the deformation of a large highly-viscous body may be analogous to the smaller scale situations, even if it is punctuated by small scale dykes. This is in agreement with the observation that large intrusions tend to be bulbous, even if they have associated dykes.

The pressure at the injection tube, at the base of the experimental device, corresponds to the gravitational pressure minus

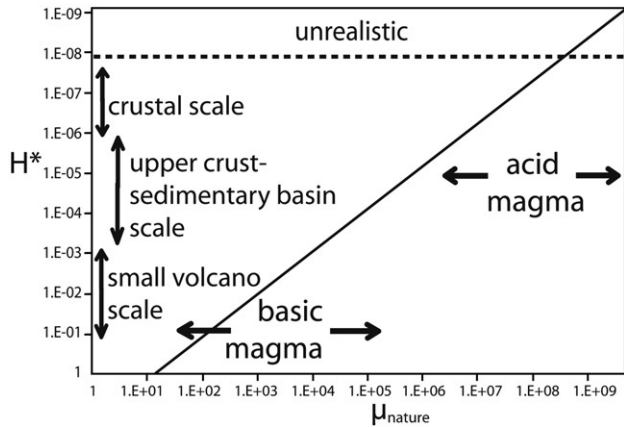


Fig. 2. Plot of the viscosity of natural magma obtained from the viscosity ratio scaling (μ^*) versus the length ratio (H^*). This shows how, by scaling the length, different scale magmatic scenarios with variable viscosity can be modeled.

the viscous drag and is about 7×10^3 Pa (Galland, 2004). The overpressure is defined by the pressure at the injection tube minus the pressure of the overburden material and is $2 \cdot 10^3$ Pa to $3 \cdot 10^3$ Pa for the bulk of experiments. These values correspond to natural overpressure of about 4 MPa and this value is within the range of estimated value of the overpressure of natural examples: 1 to 10 MPa (Rubin and Pollard, 1988).

We establish dimensionless numbers by combining the parameters listed in Table 1. Intrusion rate, intrusion velocity and gravitational acceleration are constant in our experiments. Thus, we reduce the number of variables to 9: diameter, height, density, viscosity and emplacement depth of intrusions; cohesion, density, internal angle of friction and height of host rocks. According to the Buckingham Π theorem (e.g. Middleton and Wilcock, 1994), we define 6 dimensionless numbers. Here, we only present a selection of these numbers. The three first Π -numbers (Table 1) used a ratio of geometric parameters: H_{base} (emplacement depth of cup-shaped intrusions), H_{max} (maximum height of host rocks — 30 cm), \varnothing (diameter of the intrusions) and H_{intr} (height of intrusions). Note that the Π -number values for the models are close to those of the nature, indicating that the models are appropriately scaled (Table 1).

2.3. Experimental device

For the bulk of experiments, the analogue liquid is placed in a tank connected to the base of the experimental setup by a tube 2 cm in diameter. The liquid intrudes due to the pressure difference between the reservoir and the model. Intrusion rate can be measured accurately by the drop in level of the reservoir. The reservoir has a volume 20–50 times larger than the intrusion, which means that over the model run the pressure drop is small as the top level changes only slightly. Calibrations show that the rate of extrusion with no overburden is effectively constant over the time-scale of an experiment (any change is below our measurement capability). However with overburden, the intrusion rate increases during most experiments. This is probably due to reduction in the confining pressure as the dyke rises (Rivalta and Dahm, 2006). This shows that the drop in pressure in the reservoir

is not significant in relation to other effects. The tank is placed 50 cm above the base of the model's floor for the bulk of experiments (Fig. 3).

We conducted two sets of experiments, both sets in boxes with basal dimensions of 40 cm \times 40 cm (Fig. 3). In the first set, referred to as *half box* experiments, analogue magma was intruded from the feeder tube along a wall of the box. This wall was made of glass, allowing the dyke to be observed and photographed in cross section as it grew. In the second set, referred to as *full box* experiments, the injection tube is centered at the box base, away from the walls. Surface deformation was recorded by time-lapse photography. At the end of each experiment, the model was placed in a freezer for 12 h. The Golden syrup solidifies and the intrusion was excavated and analyzed in detail.

The two experiment types have different boundary conditions, one with the dyke being intruded at an interface between a rigid material and a deformable material, and the other with the dyke being intruded far from the rigid boundary. Half box experiments enable us to observe the intrusion growth over the duration of an experiment. Full box experiments were carried out to check the validity of features observed in the half box experiments.

Our box size was chosen to fit into our deep freezer compartment. Boundary effects from the side walls of the box were minimal. Tests were made on unconfined models and in larger boxes with no difference in resulting structure. The effect of the base of the box was to allow a sill to propagate, from which a dyke eventually rose. Intrusions were also created by part-filling the box with a layer of powder and creating a Golden syrup conduit. In each case the resulting dykes were similar. If the thickness of the powder was below that of the initiation depth of cup-shaped intrusions, these formed directly from the basal sill, or conduit opening.

2.4. Experimental results

The exploratory intrusions were done with honey. High viscosity honey (200 Pa s) produced large cup-shaped intrusions at the bottom of the box. Low viscosity honey (80–140 Pa s) formed dykes (vertical sheet-like intrusions), sills (horizontal sheet intrusions), inclined sheet intrusions (with variable dip) and, sometimes, small cup-shaped intrusions fed

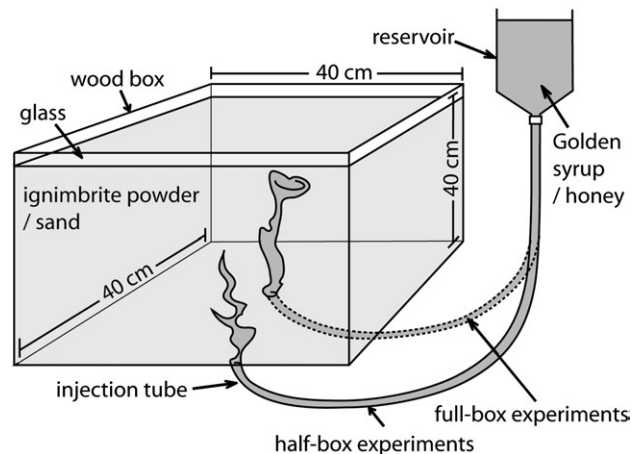


Fig. 3. Experimental device used in half box and in full box experiments.

by dykes. Golden syrup intrusions are similar in shape to honey intrusions when they have similar viscosities. At low viscosity, intrusions are thin and their development at a small-scale is easier to observe when using ignimbrite powder. For these reasons, the bulk of experiments are carried out with this set-up.

2.4.1. Dyke and sheet intrusion morphology

During half box experiments intrusions generally propagated as a thin dyke tip (0.1 cm thick) that then inflated to reach a thickness of 0.5 cm. At shallow depth (1 to 3 cm below the model surface) however, vertical intrusions remained thin and once they pierced the surface, their morphology remained fixed.

We observed that dykes did not propagate as straight vertical sheets and that the dyke tip was highly irregular. Commonly, it developed two rising branches that grew to a maximum length of 0.2 to 0.7 cm (mean value=0.4 cm) and that formed an angle of 40° to 60° to the horizontal. One of these branches generally grew at the expense of the other and the branching process continually repeated at the dyke tip. This occurred one to three times over 1 cm of propagation. For many intrusions one branch

systematically grew at the expense of the other branch, forming inclined sheet-intrusions dipping about 60° (Fig. 4a).

At depths between 30 and 7 cm two rising branches developed simultaneously and surrounded a small fragment of host material. At shallower depths (7 to 2 cm below the surface for Golden syrup intrusions), simultaneous branch growth ultimately formed a cup-shaped intrusion (see Section 2.4.2.). Some intrusions also separated into several branches along a vertical axis, forming two dykes in a single experiment. These dykes had similar lengths and the angle between them was 30° to 40° (Fig. 4a and b).

When excavating half box and full box experiments, we noticed that intrusions are thin sheet-shaped bodies covered with depressions, bulges and humps. Each of these features covered an area less than 1 cm^2 (Fig. 4c). The dyke tip also consisted of a succession of ridges and depressions.

2.4.2. Cup-shaped intrusion morphology

Cup-like intrusions developed at shallow depths for 40% of experiments (Fig. 4b–d). The development of these intrusions is well observed in half box experiments and occurs as follows. For

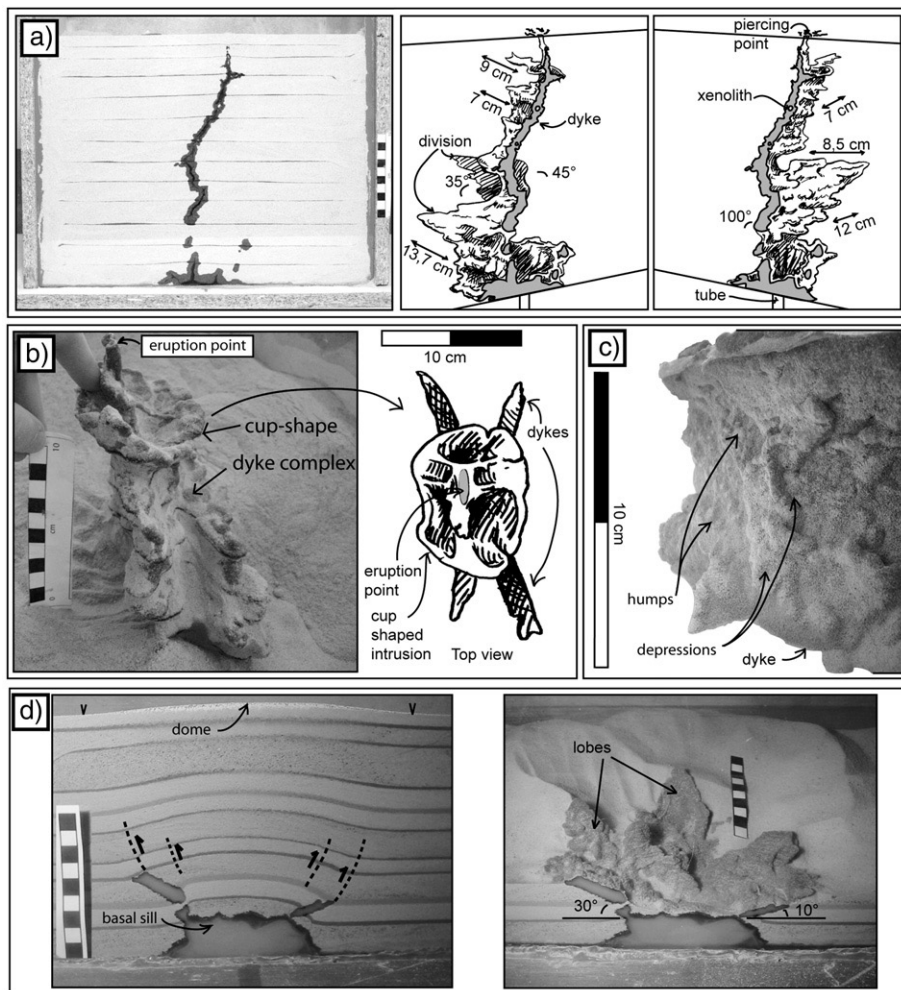


Fig. 4. Pictures and sketches of 4 experiments: (a) experiment C11 (“half box”, Golden syrup-ignimbrite, 30 cm thick), a dyke forms (b) experiment C1, (“full box”, Golden syrup, 20 cm thick), two dykes feed a cup-shaped intrusion (c) experiment E36, (“full box”, Golden syrup, 15 cm thick), a dyke forms (d) experiment E34 before and after exhumation, (“half box”, cold honey, 15 cm thick) a cup-shaped intrusion forms.

high viscosity intrusions (honey with 200 Pa s: equivalent to 10^5 Pa s in nature), intrusion formed a sill at the model base. The sand above the sill was flexed and once the ratio between the sill-length and its depth was larger than 0.5–0.6 a surface dome formed. The dome diameter was 2 to 3 times larger than the basal sill diameter. Next, rising arms forming a cup-like structure developed at the edge of the sill-like intrusion. The arms dipped 30° to 35° toward the sill and they progressively grew towards the surface (Fig. 4d). These arms induced further flexure of the country rocks. Once the intrusion horizontal diameter, defined by the rising arm edge, was equal to the surface dome diameter, the arms ceased to develop. At this stage, the central thickness of the cup-shaped intrusion increased and steep reverse faults developed, bounding the flexed dome. The dome material is moved vertically as it is progressively extruded above the cup-shaped intrusion. The cup centre thickens and changes towards a lopolith shape. A proper lopolith (flat-topped intrusion) has never been obtained during this study. This may be because of one limiting factor of our models, that in nature a small dyke exiting the magma body would freeze quickly, but we cannot halt our dykes. With dyke solidification, large scale intrusions at depth could continue to develop before they cool, and ultimately a cup-shaped intrusion could evolve into a lopolith.

For low viscosity intrusions (warm honey and Golden syrup at 50 Pa s), either no basal sill formed, or a vertical dyke formed from the sill above the injection tube. The dyke rose by forming branches. These dyke tip branches developed simultaneously at shallow depths and formed a cup-shaped intrusion (Fig. 4b). The rising branches formed an angle of 25° – 30° with the horizontal and their growth is coeval with the formation of a dome at the surface of the model. For the bulk of experiments, the vertical relief

of the dome and the intrusion thickness were of similar amplitude (Fig. 5). The dome diameter was dependant on the intrusion depth: cup-shaped intrusions emplaced at depth (13.5 cm depth for example, Fig. 4d) were overlain by domes that possessed a large diameter (20.5 cm) and cup-intrusions formed at shallower depths (5 cm for example, Fig. 4b) were overlain by smaller domes (9 cm).

The geometric relationships between the dome diameter and the intrusion depth and between intrusion diameter and depth (Fig. 5) are similar. Once the surface dome formed, its diameter was not modified by further intrusion growth. Once the intrusion reaches the surface dome diameter, the central thickness of the cup-shaped intrusion increases and steep reverse faults develop from the arms to the surface of the model, at the edge of the dome. Finally, a vertical thin dyke forms on one point of the cup-shaped intrusion (at the arm extremity usually) and follows the thrust faults toward the surface.

All the cup-shaped intrusions obtained in our experiments are divided into several arms or intrusion lobes (Fig. 4d). These intrusions possess an aspect ratio (II_1) that ranges from 0.2 to 0.35 and are circular in plan view.

2.4.3. Parameters affecting cup-shaped intrusion development

During the bulk of experiments, the intrusion rate is maintained constant. The density of Golden syrup and honey are close and so have no differential effect on intrusion development. Thus, we are able to study the effect of viscosity alone on cup-shaped intrusion. Cups are initiated at shallow depth (1 to 7 cm) when using a low viscosity analogue magma and deeper when using high viscosity analogues (15 cm; Fig. 5b). The deeper the intrusion is emplaced (II_2), the larger are its diameter (II_3) and its height (Fig. 5c). This observation is in agreement with several

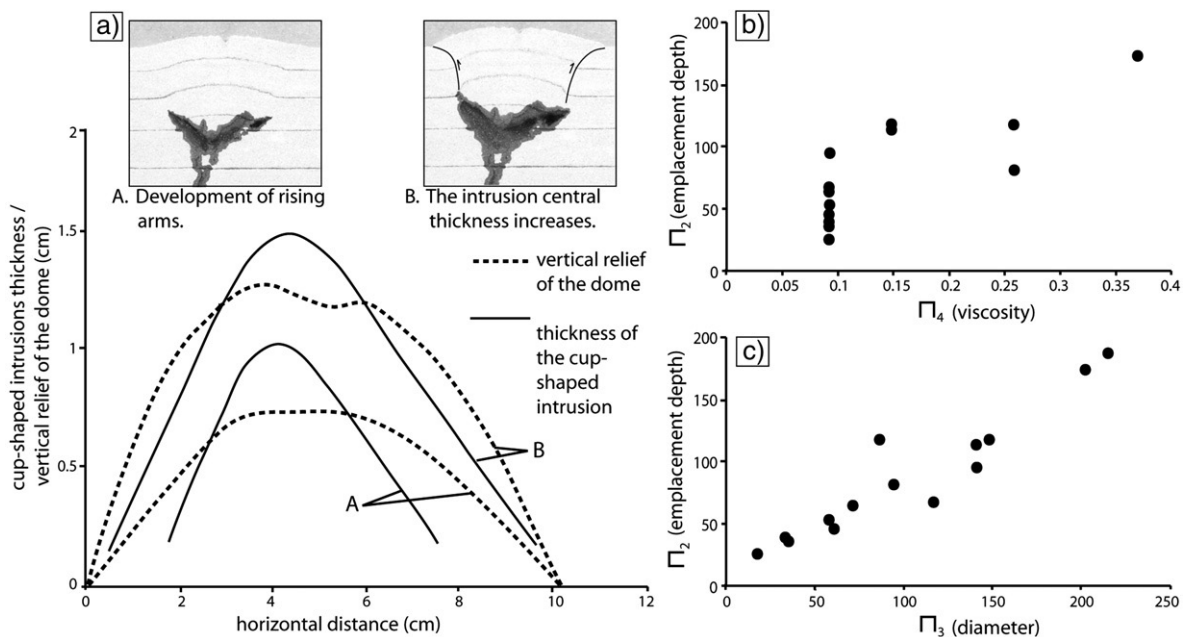


Fig. 5. (a) Comparison between the thickness of the cup-shaped intrusion and the vertical relief of the dome, the measurement has been done at two different stages of experiment C7 (half box, Golden syrup, 30 cm thick): A. at this stage, the intrusion develops its rising arms, B. the central thickness of the intrusion increases; Graphs showing the relationship between the viscosity of the intruding analogue magma and the morphology of the cup-shaped intrusions (b) II_2 (depth emplacement) versus II_4 (viscosity of cup-shaped intrusions) (c) II_2 (depth emplacement of cup-shaped intrusions) versus II_3 (diameter of cup-shaped intrusions).

authors (Roman-Berdiel et al., 1995; Kerr and Pollard, 1998; Zenzri and Kerr, 2001; Malthe-Sørenssen et al., 2004) that consider that the shapes and sizes of magma reservoirs are mainly controlled by the magma driving pressure (constant in our experiments) and by their depth of emplacement.

2.5. Discussion

2.5.1. Dyke morphology and propagation

For brittle conditions, Pollard (1973) predicted that potential shear failure at the dyke termination would be oriented at 30° to the greatest principal stress and provided a natural example of a sill with shear faults at its tip. Donnadieu and Merle (1998) observed that normal and reverse faults appear at the front of an advancing highly viscous intrusion that propagates along these faults in a manner they termed *viscous indenter* (Fig. 6).

Using the viscous indenter idea and our observations we propose that dykes can cause shear failure in their country rock and can propagate along these shears with little or limited tensional failure (Fig. 6). The following statements are derived from observation of half box experiments, where there is nearly plane strain deformation. We then consider the case of a freely deforming triaxial deformation system in the full box experiments.

2.5.1.1. Plane strain deformation. As a dyke enlarges, it pushes back the host material around it. This creates extension and stretching at the dyke tip resulting in the formation of two normal faults at the tip of the intrusion (Fig. 7a). Such features are observed with brittle indenters and highly viscous indenters (e.g. Donnadieu and Merle, 1998) and were also proposed by Pollard (1973) (Fig. 6). Numerical and analogue simulations show that extension fractures and faults should be concentrated in two zones on opposite sides of the dyke plane and converge towards the tip (Mastin and Pollard, 1988). The

ratio between the width of the surface deformation zone and the depth of the dyke tip is 2.6 (Mastin and Pollard, 1988). This value is derived from analysis of purely elastic media and could vary when considering non-elastic host material, but is near the conjugate fault type of response modeled here. Koide and Bhattacharji (1975) calculated the stress distribution around an overpressured vertically-elongated magma reservoir and predicted that such intrusion should be overlain by vertical extensional fractures and by normal faults and tension fractures dipping toward the intrusion with an angle of 45° to 60° respectively. Our models are in agreement with this analytical solution as the normal faults that develop at the tip of the dykes obtained experimentally dip 40° to 60° inward. The analogue liquid then exploits the normal faults as it is the mechanically easier option (Weertman, 1980; Donnadieu and Merle, 1998). This infiltration of the shear zones results in the formation of the two arms at the dyke tip that we observed to develop in four different ways.

1. First, one arm grew faster than the other. The liquid soon abandoned the smallest arm and the largest propagated (Fig. 7a). Repetition of this mechanism formed a sheet intrusion inclined toward the left or the right of the experiment (Fig. 4a).
2. Second, the arm enclosed a piece of host material as the tip linked after a branching, forming an inclusion (Fig. 4a).
3. Third, a central dyke appeared between the arms. This thin dyke soon enlarged and propagated. This type may be linked to the formation of a fracture related to tensional stresses created over the dyke, between the expanding arms. This suggests that both hydraulic and shear-related intrusion propagation can operate at the same time.
4. Fourth, at shallow depth (less than 7 cm for Golden syrup intrusions), the arms developed symmetrically and formed a cup-shaped intrusion (Fig. 7b).

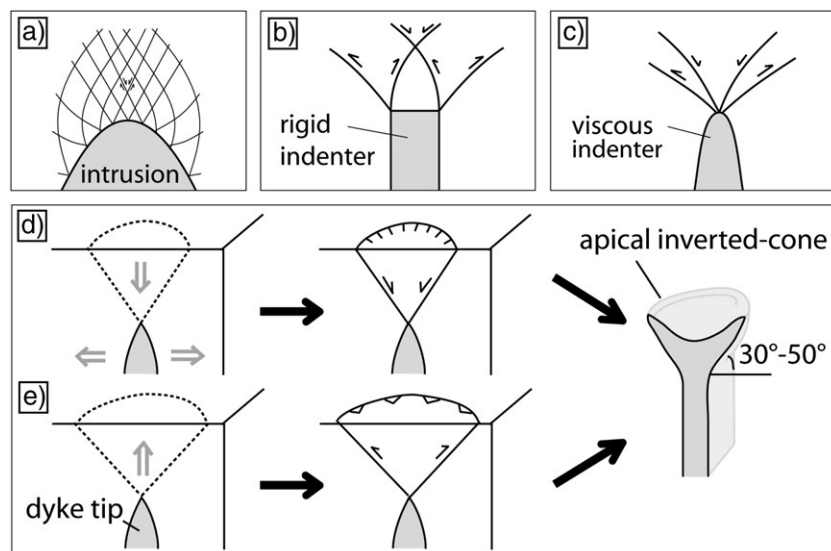


Fig. 6. Intrusion propagation mechanism by indenter and shear failure: (a) shear failure trajectories at a dyke tip, suggested by Pollard (1973), (b) fault trajectories around a rigid indenter, and (c) a viscous indenter suggested by Donnadieu and Merle (1998), (d) Our suggestion of circular normal fault trajectories over an intrusion point below cup-shaped intrusion initiation depth, (e) circular reverse fault trajectories above cup-shaped intrusion initiation depth, and the apical inverted cone dyke tip typical of the experiments and the natural examples given in Fig. 8.

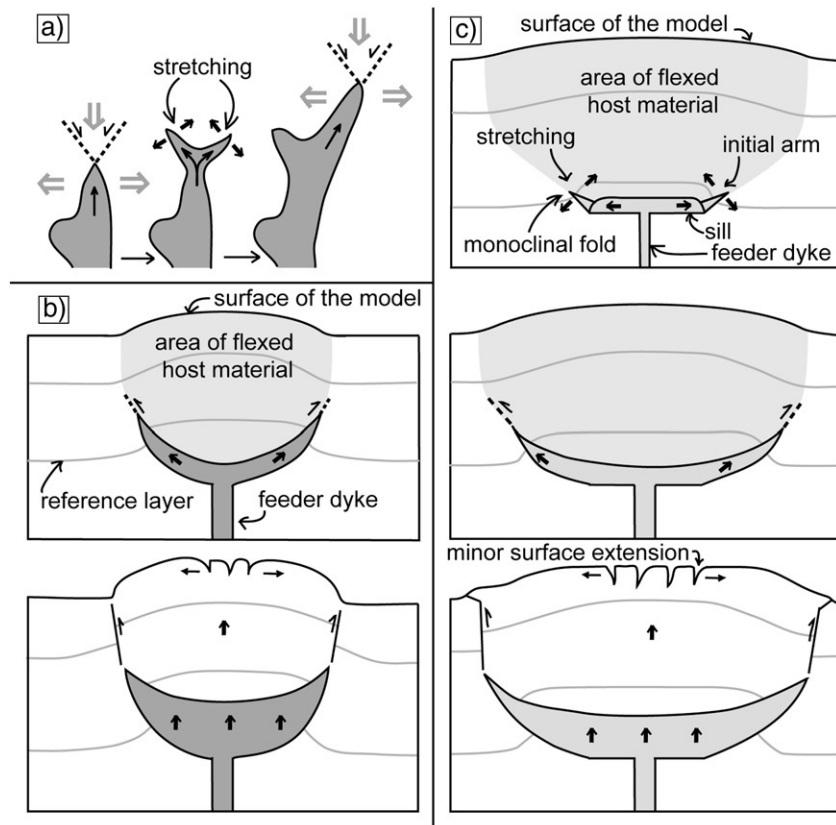


Fig. 7. Mechanisms for intrusion propagation and cup-shaped intrusion growth: (a) dyke propagates by infiltrating normal faults by repetitive branching, (b) for low viscosity intrusive liquids, a small inverted cone-like structure forms initially. Then a inverted a cup-shaped structure develops, forming a dome at the surface of the model. Ultimately, the central thickness of the intrusion increases and thrusts form above of the cup-shaped intrusion, (c) for high viscosity intrusive liquids, a sill forms, this folds the surrounding rock. The intrusion then grows up shear faults created at the fold hinge.

As a dyke propagates the small-scale features link and are partially erased. However, many abandoned arms persist and eventually formed humps on the dyke surface (Fig. 4c). The dyke tip, for example, consisted of a succession of ridges and depressions. Inclusion of host material and the irregular surface of dykes were often the only remnants of this propagation style. One important feature of this process is to create structures that are normal to the transport direction. Such types of transverse structures are common on dykes we have observed (Fig. 8), even though previous work (e.g. Pollard, 1973) only reported transport parallel structures.

2.5.1.2. Triaxial strain. A model that accounts for the full 3-D geometry of intrusions is now proposed. The dyke tip is highly irregular: it consists of a succession of humps and depressions that represents zones that have grown further than their counterparts. The humps are used as a point source of deformation: 3-D funnel-shaped normal faults develop at their tips (Fig. 6). These faults might be circular and, once infiltrated by Golden syrup, are at the origin of the formation of a cup-shaped intrusion.

The faults might also be elongated along the dyke and several could link forming an elongated ring fault, or graben, at the dyke tip. This enables the whole intrusion to migrate upward or toward the left or the right of the experiment, forming an inclined sheet intrusion (Fig. 4a). We note that the mechanism presented

here should occur all along the edge of the dyke. Thus at the dyke side the deformation can be on strike-slip faults. This enables the dyke to develop horizontally and two thin advancing arms develop at the dyke edge. These arms can develop simultaneously to form a triple branched dyke (Fig. 4a and b).

2.5.2. Cup-shaped intrusions

Cup-shaped intrusions with low and high viscosity are initiated in different ways in the models. A high viscosity intrusion (200 Pa s) first develops a sill before developing rising branches (Fig. 7b). For these intrusions, the sill flexes the country rocks once the ratio between the sill length and the sill depth is larger than 0.5–0.6. Previous work concluded that the sill is able to flex its overburden to form a laccolith once the ratio of its length and depth of emplacement is 3 (Pollard and Holzhausen, 1979; Koch et al., 1981). Our models allow non-elastic deformation to occur and this could be the reason why the ratio obtained experimentally is different from the value derived from elastic solutions.

Numerical models and field observations have also predicted that a sill should propagate out of its plane toward the free surface once the ratio of its length and depth exceeded 3 (Bradley, 1965; Pollard and Holzhausen, 1979) or 2 (Fialko, 2001). In our experiments we observe that sill development caused the roof to uplift and hence caused a forced folding of the overburden as

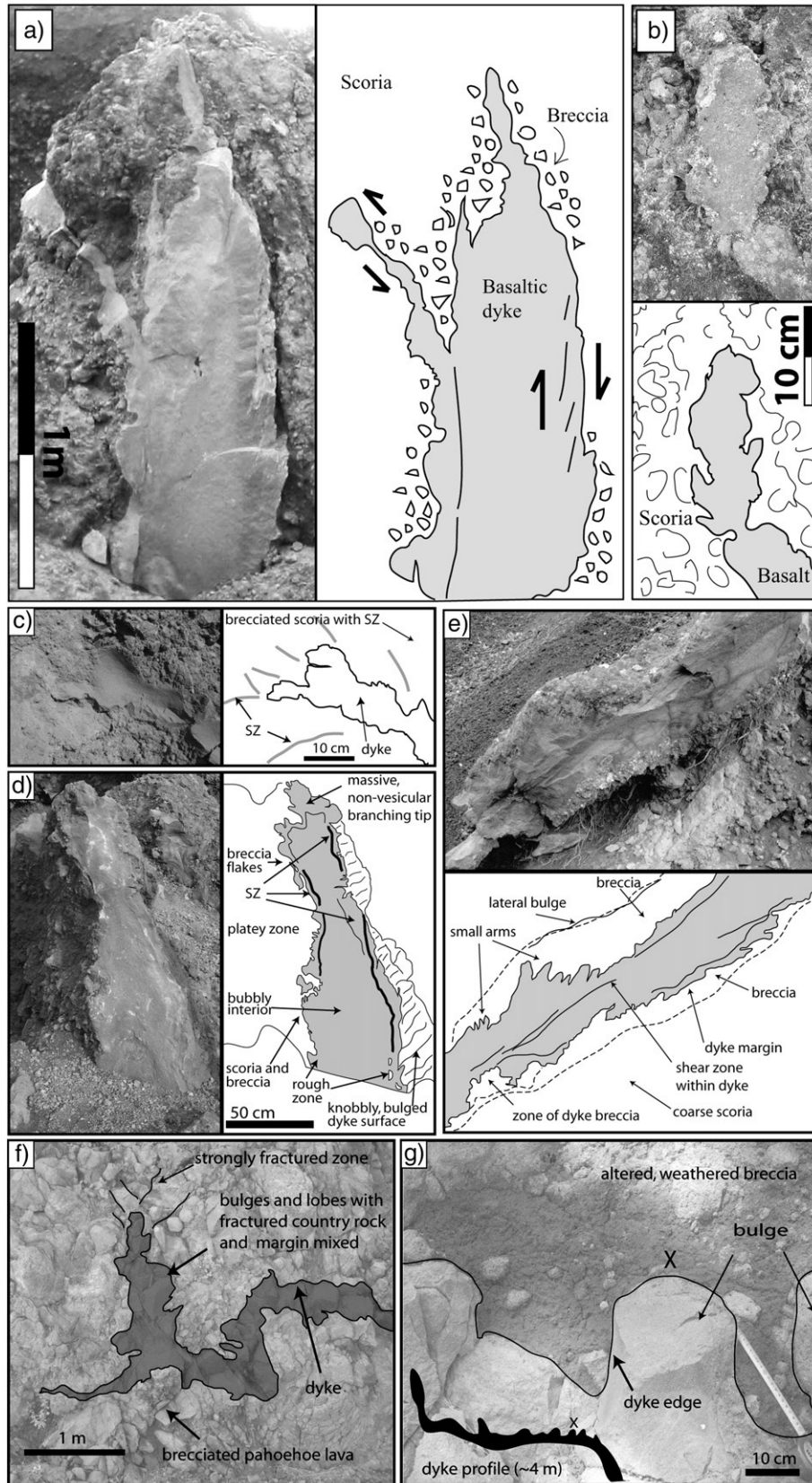


Fig. 8. Natural examples of dykes with features reproduced in the models, (a) photograph and sketch of a basaltic dyke emplaced in the scoria cone of Lemptègy (b and c) photographs and sketches of details of Lemptègy dyke tips, (d) photograph and sketch of another Lemptègy dyke, (e) photograph and sketch of an inclined dyke in the Gravenoire volcano, (f) irregular dyke intruded into brecciated lava in the northeast rift of Teide, (g) detail of the top surface bulges of a dyke intruded into altered, weathered breccia in the northeast rift of Teide.

proposed by (Pollard, 1973). In our experiments and in natural settings (e.g. Stearns, 1978) such forced folds form at shallow depth. As the curvature of the folded overburden increases, either by inflation or lateral sill propagation as a thick mass, the stretching at the fold hinge becomes excessive and fractures or shear faults form on the convex part of the fold. This mechanism is proposed by Thomson (2007) to create tension fractures that allow upward migration of magma from sills. In our models, the analogue magma infiltrates shear bands created on the fold and the rising arms develop along these. This mechanism does not happen simultaneously at every point of the sill extremity, resulting in the growth of several separated arms from the edge of the sill (see Fig. 4d) and this is also reported by Thomson (2007). These arms develop independently and coalesce, forming different intrusion-lobes (Fig. 4d). Once the arms are initiated they create and follow a shear zone with an inverse sense of movement (Fig. 7c) as described below for low viscosity intrusions.

As intrusions rise, the overburden pressure decreases and thus the vertical stress reduces. This corresponds to one of the principle stress axes in the model. At shallow depth (7 cm depth for Golden syrup experiments), this vertical principal stress becomes the smallest and the intrusion is able to uplift the host material along a conjugate pair of reverse faults. Thus, the small apical cone that commonly forms at the dyke tip (Fig. 6a) of low viscosity intrusions (Golden syrup and warm honey) develops symmetrically to form a cup-shaped intrusion (Fig. 7b). The intrusion arms develop in shear zones with a reverse sense of movement that delimits the flexed analogue country rocks.

Cup-shaped intrusions obtained in our experiments are inverted cones. They possess neither a large sill base nor an outer sill, meaning that these intrusions are not strict analogues of natural saucers. However, like natural saucers, they form near the surface and are surmounted by a dome. The main difference in genesis is probably the role of layered crust in creating sills for saucers.

Like the analogue dykes, the cup-shaped intrusions obtained here show highly irregular surfaces. Such features had been recognized in the field on both dykes and sills (Pollard and Johnson, 1973; Francis, 1982; Rickwood, 1990) and on seismic profiles for saucers (Thomson and Hutton, 2003). Irregularities have also been recognized on saucers of the Karoo basin. It has been argued (Polteau et al., 2005) that such surface irregularities are due to the thermal contraction of the chilled saucer margin. As such processes are not reproduced in the experiments presented here, we cannot test this hypothesis, but suggest that our branching propagation model may equally explain these structures.

3. Comparison with natural examples

3.1. High level dyke emplacement in scoria cones

Near-surface (<1 km) dyke emplacement can be observed on rift zones and in scoria cones. Here we provide examples from the Chaîne des Puys (French Massif Central) and two examples from the north-east rift of Teide (Canary Islands). The Puy de Lemptègy and Gravenoire volcanoes are deeply quarried scoria cones and they provide excellent sites to observe dykes at a shallow within-edifice level. The Lemptègy volcano was built by two eruptions

(Lemptègy I and II), 30,000 years ago, Gravenoire dates from about 75,000 years ago. The deposits consist of basaltic to trachyandesitic scoria, lava flows and in both cases a dense intrusive complex is preserved: cryptodomes, dykes and spatter cones form well-preserved 3-D outcrops. Dykes were emplaced near the surface (<100 m) in a dominantly coarse scoria.

Fig. 8a shows the thin tip (0.1 m wide) of a 0.7 m wide dyke. This massive dyke is surrounded by crushed scoria that is mixed with brecciated dyke material in a diffuse contact zone. The right edge of the dyke is smooth and shows evidence of shear displacement, such as tension gashes, Riedel shear faults, parallel laminations and striations. The left side of the dyke is highly irregular, showing bulges that are very similar to those seen in the analogue models. This side also has a shear zone, but it is within the dyke (seen as a distinct line on Fig. 8a). This shear zone is associated with a welded breccia within the massive dyke. The shear zone passes up into a thin branch of the dyke that extends to the left. There are several such branches on the dyke that are similar to the branches observed in the models. The dyke tip of the left hand branch is shown in Fig. 8b. This shows several small arms and a bulbous head. Another part of the dyke tip is shown in Fig. 8c. This tip is surrounded with brecciated scoria, with finer bands, and may represent shear bands formed during propagation. Another dyke is shown in Fig. 8d. This dyke has well exposed shear bands that are intermittently present on the dyke margins. It has a knobby, bulbous, branching tip and a similarly textured dyke side surface.

Fig. 8e shows an inclined dyke from the Gravenoire scoria cone. This dyke is aligned with a well formed breccia zone ahead of its tip. The dyke is surrounded in crushed scoria, and has pronounced ridges, or lateral bulges on the exposed side that correspond to small arms within the dyke margin. The lower side contains pockets of brecciated dyke material and has fewer arms. The last two images in Fig. 8 (Fig. 8f and g) are taken from the northeast rift of Teide. The first shows a thin dyke intruded into brecciated pahoehoe. The irregular dyke has repeated arms and the vertical termination is associated with a strongly fractured zone. The last example (Fig. 8g), shows the top edge of a low angle dyke that cuts through an altered, weathered breccia. Bulbous dyke arms are consistent with a viscous indenter type of displacement of the country rock. Further from this image, the dyke swings to vertical, on an extended bulge (see silhouette of dyke trace on Fig. 8g).

The ensemble of dyke examples shown here have the characteristic morphology of those seen in the analogue models, with arms, bulges and lateral ridges normal to propagation direction. The breccias formed at their tips and occasional shear zones are also in agreement with viscous indenter-type propagation.

3.2. A volcano-scale cup shaped intrusion: Ardnamurchan volcanic centre

The Ardnamurchan peninsula, Scotland, is a deeply eroded volcanic center. Three successive nested gabbroic bodies dated at 61 Ma to 57 Ma were emplaced (Walker, 1975). The Mesozoic sedimentary rocks have been updomed and dip away from the intrusive complex at about 30° (Richey et al., 1930). The

emplacement depth of the three successive Ardnamurchan intrusions is roughly constrained by the presence of the prevolcanic surface, and is probably 1–2 km. The layering of center 2 hypersthene gabbro dips inward and the base of the intrusion has probably a conical shape (Wells, 1953). A recent AMS (Anisotropy of Magnetic Susceptibility) study has shown that the gabbroic bodies of center 3 (and potentially also centers 1 and 2) have a lopolith shape (O'Driscoll et al., 2006; Fig. 8). We propose that these gabbros have been emplaced with a cup-shape and have domed their country rocks. These intrusive complexes may represent the late stage evolution of cup-shaped intrusions, where the central thickness of the intrusion increases. In our model, lopoliths do not need a sagging episode to form as argued by O'Driscoll et al. (2006). They simply are emplaced with a cup-shape at relatively shallow depth.

Numerous doleritic cone-sheets, dykes and sills are preserved at Ardnamurchan. These are sheet-like bodies and have smooth boundaries. Their morphology contrasts strongly with the dykes obtained in our experiments. Ardnamurchan dykes and cone-sheets are thought to have been emplaced into fault zones and fractures related to the formation of the lopolith (Speight, 1972; Fjeldskaar Lotveit and Gudmundsson, 2003). They represent a second type of dyke emplacement that has not been modeled here. We have investigated the faulting of host-rocks by magma, but we have not modeled the emplacement of magmatic liquid into pre-existing fault-zones.

3.3. Circular volcano complexes

Throughout arcs and especially in the Central Andes there are groups of volcanoes distributed in circles or crescents (Fig. 9).

Such features normally comprise a set of four to ten centers, sometimes with a central volcano. In addition, several calderas are found with volcanoes distributed around the margin. A good example of a caldera with a ring of volcanoes the Karymski area in Kamchatka (Belousov et al., 2005). Exposed batholiths sometimes also have ring structures. We suggest that these surface rings of volcanoes are possibly fed by deep intrusions that develop into cup-shaped bodies. The intrusions could be much more complex than our single intrusion type and several pulses of intrusion could create a complex multiple ring intrusion.

The production of such large scale cup-shaped intrusions can be modeled with our set up if the viscosity scaling and length scaling is increased, as indicated above. In this case the magma analogue represents a highly viscous crystal mush, and the brittle powder the brittle crust. Such models cannot deal with large variations in magma viscosity (the growing intrusions may contain low viscosity magmas as well), but it is possible to envisage two modes of deformation, one a slow growth of the main intrusion and the other the short scale punctuated injection of low viscosity dykes. To take a natural analogous system: in a fault zone ductile deformation can create shear zones, where punctual tension gashes and veins can form in transient high strain events.

Examples of such ring structures in the Andes are Irruputuncu, N Chile (Fig. 9), the Yucumane range, Peru and the Aucanquilcha group of volcanoes, Chile (Klemetti and Grunder, 2008). The Azufre–Lastaria group is interesting as it is the site of a large crustal dome and active uplift (Froger et al., 2007). This dome has also a localized topographic anomaly on Lastaria, which may indicate the present focus of activity from a cup-shaped intrusion system.

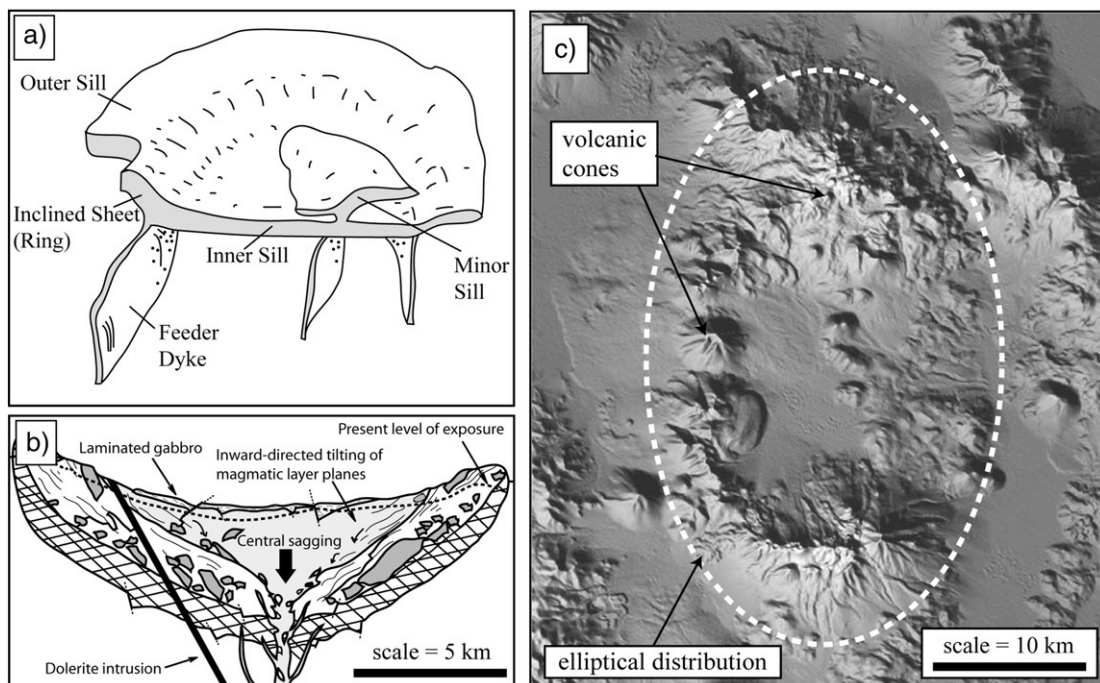


Fig. 9. (a) sketch of a typical saucer-shaped dolerite intrusion (after Chevallier and Woodford, 1999), showing the resemblances and differences between cup-shaped and saucer shaped intrusions, (b) cross-section of the center 3 gabbroic lopolith of Ardnamurchan (after O'Driscoll et al., 2006), showing its cup-shaped geometry, (c) circular arrangement of volcanic edifices at Irruputuncu (N Chile). Such an arrangement of edifices may be related to the development of a crustal-scale cup shaped intrusions.

4. Concluding remarks

The aim of this study is to model near-surface intrusions emplaced into a granular material. Intrusions obtained here propagate mainly by shear faulting of the host material and infiltration into these faults. Dykes obtained are roughly vertical intrusions that show an irregular surface and form. We argue that they are a direct analogue of near-surface dykes emplaced, for example, in scoria cones such as Lemptègy. In our models, as an intrusion develops, funnel-shaped normal faults open at the dyke tip. The intrusion thus develops by successive shear band or shear fault formation and infiltration of these fault zones by stretching the deformed rock. Shear failure is associated with low rock cohesion (i.e. low shear strength) and a broad dyke tip that generates a viscous indenter. At higher cohesion (or shear strength) and with thinner dyke tips (e.g. when infiltrating fractures) the rock may fail in tension and hydraulic fractures can form instead of shear faults.

Cup-shaped intrusions develop at variable depths in our experiments, dependant on the analogue viscosity. The highest viscosity produced the deepest cup-shaped intrusions and, the deeper the intrusion formed, the larger it grew. Like natural saucer-shaped intrusions described in sedimentary basins, cup-shaped intrusions flex the host material above them and form a dome at the surface. When using a high-viscosity analogue magma (honey), cup-shaped intrusions possess a sill base much shorter than the inner sill of natural saucer-shaped intrusions. In natural examples, sills infiltrate sub-horizontal weakness zones as, for example, the interfaces between sedimentary strata and, as an interface has not been modeled here, proper saucers and sills were not obtained, or expected. The cup-shaped intrusions obtained with a low viscosity analogue magma (warm honey, golden syrup) do not possess a sill base. They initially form by infiltrating fault zones that open at the dyke tip and their development forms a forced fold in the overburden. Then, these intrusions develop in the reverse faults that delimit the flexed host material. Their late evolution, which consists of the increasing of their central thickness, provides a mechanism for the formation of lopolith intrusions.

The results from the analogue modeling agree with field observations on dykes such as those in Lemptègy that clearly show strong brecciation of the host rock, the advance of the intrusion on side-parallel shears and the presence of side structures consistent with the bifurcating of a dyke tip along shear zones. While hydraulic fracturing unquestionably occurs under many circumstances, viscous indenter-related shear failure is also a major dyke propagation process in brittle rocks. Viscous indenter-related shear failure also provides a genetic mechanism for the shape and evolution of cup-shaped intrusions, saucer-sills and lopoliths.

Acknowledgements

The authors wish to thank G. Ernst and M. Kervyn for their advice and corrections; V. Troll and the postgraduate students of Trinity College, Dublin, for their constructive reflections and O. Merle for his help. Tate and Lyle generously provided the Golden

syrup. Lemptègy quarry (www.auvergne-volcan.com) generously excavated dykes for us.

References

- Bradley, J., 1965. Intrusion of major dolerite sills. *Trans. Royal Soc.* 3, 27–55.
- Belousov, A., Walter, T.R., Troll, V., 2005. Large-scale failures on domes and stratovolcanoes situated on caldera ring faults: sand box modeling and natural examples from Kamchatka, Russia. *Bull. Volcanol.* 67, 457–4680.
- Cecchi, E., van Wyk de Vries, B., Lavest, J.M., 2004. Flank spreading and collapse of weak-cored volcanoes. *Bull. Volcanol.* 67 (1), 72–91.
- Chevallier, L., Woodford, A., 1999. Morpho-tectonics and mechanism of emplacement of the dolerite rings and sills of the western Karoo, S Africa. *S. Afr. J. Geol.* 102, 43–54.
- Donnadieu, F., Merle, O., 1998. Experiments on the indentation process during cryptodome intrusions: new insights into Mount St. Helens deformation. *Geology* 26 (1), 79–82.
- Fialko, Y., 2001. On origin of near-axis volcanism and faulting at fast spreading mid-ocean ridges. *Earth Planet. Sci. Lett.* 190, 31–39.
- Fjeldskaar Lotveit, I., Gudmundsson, A., 2003. Aperture variation and fault–dyke interaction during dyke propagation in a layered rift zone. Conference abstract, EGS-AGU-EUG Joint assembly, abstract, pp. EAE03–A-09684.
- Francis, E.H., 1982. Magma and sediment—I. Emplacement mechanism of late Carboniferous tholeiite sills in northern Britain. *J. Geol. Soc. Lond.* 139, 1–20.
- Froger, J.-L., Remy, D., Bonvalot, S., Legrand, D., 2007. Two scales of inflation at Lastarria–Cordon del Azufre volcanic complex, central Andes, revealed from ASAR-ENVISAT interferometric data. *Earth Planet. Sci. Lett.* 255, 148–163.
- Galland, O., 2004. Interactions mécaniques entre la tectonique compressive et le magmatisme: expériences analogiques et exemple naturel, PhD dissertation, Renne university, France.
- Galland, O., Cobbold, P.R., Hallot, E., de Bremond d’Ars, J., Delavaud, G., 2006. Use of vegetable oil and silica powder for scale modelling of magmatic intrusion in a deforming brittle crust. *Earth Planet. Sci. Lett.* 243, 786–804.
- Hansen, D.M., Cartwright, J., 2006. The three-dimensional geometry and growth of forced folds above saucer-shaped igneous sills. *J. Struct. Geol.* 28, 1520–1535.
- Heimpel, M., Oison, P., 1994. Buoyancy-driven fracture and magma transport through the lithosphere: models and experiments. In: Ryan, M.P. (Ed.), *Magmatic systems*, pp. 223–240. Chap. 10.
- Holohan, E., van Wyk de Vries, B., Troll, V., 2007. Analogue models of caldera collapse in strike–slip tectonic regimes. *Bull. Volcanol.* 70 (7), 773–796, doi:10.1007/s00445-007-0166-x (on line first).
- Hubbert, M.K., 1937. Theory of scale models as applied to the study of geologic structures. *Geol. Soc. Am. Bull.* 48, 1459–1520.
- Hubbert, M.K., Willis, D.G., 1957. Mechanics of hydraulic fracturing. *J. Pet. Technol.* 9 (6), 153–168.
- Hyndman, D.W., Alt, D., 1987. Radial dikes, laccoliths, and gelatin models. *J. Geol.* 95, 763–774.
- Jaeger, C.M., 1972. *Rock Mechanics and Engineering*. Cambridge University Press, Cambridge.
- Kerr, A.D., Pollard, D.D., 1998. Toward more realistic formulations for the analysis of laccoliths. *J. Struct. Geol.* 20 (12), 1783–1998.
- Klemetti, E.W., Grunder, A.L., 2008. Volcanic evolution of volcano Aucanquilcha, a long-lived dacite volcano in the Central Andes of northern Chile. *Bull. Volcanol.* 70 (5), 633–650, doi:10.1007/s00445-007-0158-x (on line first).
- Koch, F.G., Johnson, A.M., Pollard, D.D., 1981. Monoclinical bending of strata over laccolithic intrusions. *Tectonophysics* 74, T21–T31.
- Koide, H., Bhattacharji, S., 1975. Formation of fractures around magmatic intrusions and their role in ore localization. *Econ. Geol.* 70, 781–799.
- Lister, J.R., Kerr, R.C., 1991. Fluid-mechanical models of crack propagation and their application to magma transport in dykes. *J. Geophys. Res.* 96 (B6), 10049–10077.
- Malthe-Sørenssen, A., Planke, S., Svenson, H., Jamveit, B., 2004. Formation of saucer-shaped sills. In: Petford, N., Breitzkreuz, C. (Eds.), *Physical geology*

- of high-level magmatic systems. Geological Society of London Special Publication, vol. 234, pp. 215–227.
- Mastin, L.G., Pollard, D.D., 1988. Surface deformation and shallow dike intrusion processes at Inyo Craters, Long Valley, California. *J. Geophys. Res.* 93 (B11), 13221–13235.
- Merle, O., Borgia, A., 1996. Scaled experiments of volcanic spreading. *J. Geophys. Res.* 101 (B6), 13805–13817.
- Middleton, G.V., Wilcock, P.R., 1994. *Mechanics in the earth and environmental sciences*. Cambridge University Press.
- Morris, G.A., Hutton, D.H.W., 1993. Evidence for sinistral shear associated with the emplacement of the early Devonian Etive dyke swarm. *Scott. J. Geol.* 29, 69–72.
- O'Driscoll, B., Troll, V.R., Reavy, J., Turner, P., 2006. The Great Euclite intrusion of Ardnamurchan, Scotland: re-evaluation of the ring-dyke concept. *Geology* 34, 189–192.
- Petford, N., Cruden, A.R., McCaffrey, K.J.W., Vigneresse, J.L., 2000. Granite magma formation, transport and emplacement in the Earth's crust. *Nature* 408, 669–673.
- Pollard, D.D., 1973. Derivation and evolution of a mechanical model for sheet intrusions. *Tectonophysics* 19, 233–269.
- Pollard, D.D., Holzhausen, G., 1979. On the mechanical interaction between a fluid-filled fracture and the Earth's surface. *Tectonophysics* 53, 27–57.
- Pollard, D.D., Johnson, A.M., 1973. Mechanics of growth of some laccolith intrusions in the Henry Mountains, Utah. Part II. *Tectonophysics* 18, 311–354.
- Polteau, S., Planke, S., Ferré, E.C., Svensen, H., Malthe-Sørensen, A., Neumann, E.-R., Podladchikov, Y., 2005. Emplacement mechanisms of saucer-shaped sill intrusions as inferred from detailed field work and AMS analyses of the Golden Valley Sill Complex, South Africa. conference abstract, Geological Society of America Annual meeting, abstract, p. 92339.
- Ramberg, H., 1981. *Gravity, deformation and the Earth's crust*. Academic Press, London.
- Richey, J.E., Thomas, H.H., Bailey, E.B., Radley, E.G., Dixon, B.E., 1930. The geology of Ardnamurchan, north-west Mull and Coll. *Memoir of the Geological Survey, U.K. Scotland*.
- Rickwood, P.C., 1990. The anatomy of a dyke and the determination of propagation and magma flow. In: Parker, A.J., Rickwood, P.C., Tucker, D.H. (Eds.), *Mafic dykes and emplacement mechanisms*. Balkema, Rotterdam, pp. 81–100.
- Rivalta, E., Dahm, T., 2006. Acceleration of buoyancy-driven fractures and magmatic dikes beneath the free surface. *Geophys. J. Int.* 166, 1424–1439.
- Roman-Berdiel, T., Gapais, D., Brun, J.P., 1995. Analogue models of laccolith formation. *J. Struct. Geol.* 17, 1337–1346.
- Rubin, A.M., Pollard, D.D., 1988. Dike-induced rift zones in Iceland and Afar. *Geology* 16, 413–417.
- Schellart, W.P., 2000. Shear test results for cohesion and friction coefficients for different materials: scaling implications for their usage in analogue modelling. *Tectonophysics* 324, 1–16.
- Speight, J.M., 1972. The form and structure of the Tertiary dyke-swarms of Skye and Ardnamurchan. Doctoral dissertation, University of London.
- Spence, D.A., Turcotte, D.L., 1985. Magma-driven propagation of cracks. *J. Geophys. Res.* 90 (B1), 575–580.
- Spence, D.A., Turcotte, D.L., 1990. Buoyancy-driven magma fracture: a mechanism for ascent through the lithosphere and the emplacement of diamonds. *J. Geophys. Res.* 95 (B4), 5133–5139.
- Stearns, D.W., 1978. Faulting and forced folding in the Rocky Mountains foreland. *Geol. Soc. Am. Mem.* 151, 1–37.
- Takada, A., 1994. Development of a subvolcanic structure by the interaction of liquid filled cracks. *J. Volcanol. Geotherm. Res.* 62, 207–224.
- Thomson, K., 2007. Determining magma flow in sills, dykes and laccoliths and their implications for sill emplacement mechanisms. *Bull. Volcanol.* 70, 183–201.
- Thomson, K., Hutton, D., 2003. Geometry and growth of sill complexes: insights using 3D seismic from the North Rockall Trough. *Bull. Volcanol.* 66, 364–375.
- Voight, B., 2000. Structural stability of andesite volcanoes and lava domes. *Philos. Trans. R. Soc. Lond.* 358, 1663–1703.
- Walker, G.P.L., 1975. A new concept of the evolution of the British Tertiary intrusive centers. *J. Geol. Soc. Lond.* 131, 121–141.
- Weertman, J., 1980. The stopping of a rising, liquid-filled crack in the earth's crust by a freely slipping horizontal joint. *J. Geophys. Res.* 85, 967–976.
- Wells, M.K., 1953. The structure and petrology of the hypersthene-gabbro intrusion, Ardnamurchan, and the problem of net-veining. *J. Geol. Soc. Lond.* 109, 367–397.
- Zenzi, H., Kerr, L.M., 2001. Mechanical analyses of the emplacement of laccoliths and lopoliths. *J. Geophys. Res.* 106, 13781–13792.